^2H NMR Line Shapes and Spin−Lattice Relaxation in $Ba(ClO_3)_2 \cdot {}^2H_2O$

Joanna R. Long, Rainer Ebelhäuser, and R. G. Griffin*

Francis Bitter Magnet Laboratory and Department of Chemistry, Massachusetts Institute of Technology, Cambridge, Massachusetts 02139

Received: July 15, 1996; In Final Form: December 3, 1996[⊗]

Solid-state deuterium NMR measurements were used to characterize the flipping motion of the water molecule in barium chlorate monohydrate, $Ba(ClO_3)_2 \cdot {}^2H_2O$. In particular, temperature-dependent quadrupole echo line shapes, their τ dependence and spectral intensities, and the anisotropy of the spin−lattice relaxation observed in inversion recovery experiments permit measurement of the 2-fold flipping rates. These were studied as a function of temperature and yield an activation energy $E_a = 30$ kJ/mol and pre-exponential factor $A_0 = 1.5 \times 10^{14}$, which are typical for molecular motion constrained by hydrogen bonds of moderate strength. A discussion of experimental considerations is also presented.

Introduction

Pulsed deuterium NMR, in combination with line shape simulations, is a powerful tool for investigating dynamic processes in solid and semisolid materials.[1,2] With this technique details on the rate and mechanism of anisotropic molecular motion are available from studies of line shapes that arise from the deuterium quadrupole interaction[3]. The size of this interaction is 170−250 kHz, and therefore, other anisotropic nuclear spin interactions, such as the dipole−dipole coupling and chemical shift, are relatively small and do not have to be considered explicitly for interpreting the spectral line shapes or spin−lattice relaxation. To investigate processes with rates between 10^3 s^{-1} (slow exchange) and 10^8 s^{-1} (fast exchange), the temperature dependence of quadrupole echo spectra and the dependence on pulse spacing, τ, can be employed.[4−6] Particularly dramatic changes in powder line shapes and spectral intensities are observed when the rates of motion are on the order of the quadrupole coupling constant $\sim 10^4 - 10^7$ s^{-1}. For faster motions, in the regime $10^8 - 10^{11}$ s^{-1}, the anisotropy of the spin lattice relaxation observed in inversion recovery experiments can be used.[7,8] This latter experiment overlaps with the upper end of the time scale of quadrupole echo measurements and in addition permits observation of faster motions where the quadrupole echo line shape is insensitive to changes in the rate of molecular reorientation. For both the quadrupole echo and inversion recovery techniques, information on the rate and mechanism of molecular motion is extracted by fitting experimental spectra with theoretical line shapes.

Generally, the theoretical spectra are calculated on the basis of a dynamic model, assuming particular values for the number of sites involved in the motional process, their populations and relative electric field gradient (EFG) tensor orientations, and the exchange rates among the sites. A particular dynamic model should be consistent with all the spectroscopic line shape data that are available. Thus, testing the applicability of a model requires careful analysis of the line shapes and intensity of quadrupole echo spectra as a function of temperature and of the solid echo pulse delay. Furthermore, one must be able to simulate the anisotropic spin−lattice relaxation recorded by the inversion recovery experiment using this model.

In the past few years, there have been several ^2H NMR studies of simple and complex molecules that have demonstrated many of the essential features expected in ^2H quadrupole echo line shapes. For instance, phenylalanine and tyrosine aromatic side chains have been shown to exhibit two-site flips,[9−11] proline ring motions have been observed,[12] and spectra of methyl and ammonium groups display line shapes consistent with 3-fold motion.[13−17] In addition, other applications have focused on more complex systems such as polymers,[18−21] proteins,[22] and lipid bilayers [23−26] that, in general, exhibit complex line shapes. For example, polymers commonly exhibit distributions of correlation times and proteins can have multiple sites that display a range of dynamic behaviors. In lipid bilayers multiple motions can occur at different rates and therefore lead to complicated spectra. Thus, despite the relatively large number of ^2H NMR studies of molecular dynamics, there is a paucity of cases where it has been possible to unambiguously confirm the correctness of the line shape and T_1 calculations. It is this fact that provided the primary motivation for the experiments described here.

To test the line shape calculations, we desired a molecule that would exhibit relatively simple molecular motions. In addition, the material should display a single phase, with a single dynamically distinct site. Finally, it is useful to have a system where the rates can be varied from $10^4 - 10^7$ s^{-1}, for instance at low temperatures where the quadrupole echo line shapes will be affected, to $10^8 - 10^{11}$ s^{-1} at higher temperatures, where T_1 and T_1 anisotropies will change. The simple hydrates are excellent candidates for this type of study. Many of these substances have been crystallized and their structure and phase behavior are well characterized.[27−30] In addition, the H_2O molecules of hydration exhibit 2-fold flips about the HOH bisector at rates that can be varied by controlling the temperature. Thus, at low temperatures the motion can be in the regime appropriate for quadrupole echo experiments, and since the molecules are relatively small and can therefore move rapidly at higher temperatures, the anisotropy of the T_1 will be affected. Finally, hydrates are easily labeled simply by recrystallization from D_2O.

Experimental Section

Sample Preparation. Single crystals of $Ba(ClO_3)_2 \cdot {}^2H_2O$ were grown by slow evaporation of a saturated solution of barium chlorate in D_2O at room temperature. The dried crystals were crushed to form a powder that was sealed in a 5 mm sample tube.

[⊗] Abstract published in *Advance ACS Abstracts,* January 15, 1997.

S1089-5639(96)02116-0 CCC: $14.00

NMR Spectroscopy. The NMR measurements were performed on a home-built spectrometer operating at a deuterium frequency of 61.05 MHz using quadrature detection and a dwell time of 0.5 μs. The $\pi/2$ pulse length was 1.6−2.0 μs. A phase-cycled quadrupole echo sequence was employed to observe τ-dependent and temperature-dependent spectra. The quadrupole echo pulse spacing varied between 30 and 200 μs. Partially relaxed spectra were recorded with an inversion recovery sequence, where Zeeman magnetization was inverted with a π pulse. After a recovery delay of time t_1, Z-magnetization was monitored by a quadrupole echo sequence. To guarantee the fidelity of the ^{2}H NMR line shapes, the recycle delays employed were typically 6 times T_1 for the quadrupole echo experiments and 12 times T_1 for the inversion recovery sequence.

Powder Line Shape Calculations. The line shape calculations discussed below account for anisotropic transverse and longitudinal relaxation, as well as finite pulse width effects. The details of the simulations are explained elsewhere.[8] Given the simplicity of this system, correlation functions for $\eta \neq 0$ were also included in the relaxation calculation. In the rigid lattice limit ($T \approx -120$ °C), deuterons in $Ba(ClO_3)_2 \cdot {}^2H_2O$ exhibit a quadrupole coupling constant (e^2qQ/h) = 244 kHz and an asymmetry parameter $\eta = 0.074$.[31] As the temperature is increased, vibration attenuates the quadrupole coupling constant and averages the asymmetry. If the water molecule is not flipping, it vibrates with frequencies on the order of 10^{13} s^{-1}.[32] However, this is much higher than the Larmor frequency employed in our experiments and should have little direct effect upon the observed spin−lattice relaxation, but as stated above, an oscillatory motion of the water molecule about the bisector leads to a decrease of the quadrupole coupling constant proportional to the amplitude of angular oscillation. Both the quadrupole coupling constant and asymmetry parameter were studied as a function of temperature in the single-crystal experiments of Chiba and co-workers. Their values were used in the present study. Since the deuteron sites are identical, the equilibrium population of each is one-half. A jump angle of 110.7° was used in close agreement with neutron diffraction analysis.[33] The spectra discussed below demonstrate that deviations in the D−O−D angle from the tetrahedral angle and the asymmetry of the static **EFG** tensor compensate for one another to yield an $\eta \cong 1$ spectrum in the fast exchange limit.

The pulse widths, quadrupole echo pulse spacing, and the delay in the inversion recovery sequence are input parameters dictated by the experiment. To account for other relaxation mechanisms, a homogeneous transverse relaxation time was introduced in the calculation by exponentially broadening the line from each crystallite subspectrum by $1/(\pi T_2^*) = 1$ kHz. This value is based on the measurement of T_2 in the fast motion limit (data not shown). This is somewhat shorter than usually observed in deuterium spectra and can be attributed to the dipole coupling between the deuteriums in the water molecule, which is unattenuated by 180° flips. Thus, the only unknown parameter in this simulation was the exchange rate, which was adjusted to provide satisfactory agreement between experimental and calculated spectra.

Results and Discussion

Deuteron Quadrupole Echo Line Shapes. In Figure 1 ^{2}H NMR quadrupole echo spectra of $Ba(ClO_3)_2 \cdot {}^2H_2O$ are shown as a function of temperature between −119 and 18 °C, together with simulated spectra for a tetrahedral jump between two sites of equal population. In a manner that will be described below, the rate constants for some of these simulations were obtained from the inversion recovery experiment (except for the low-temperature spectrum at −119 °C), where the exchange rates can be determined with high accuracy. In particular, at each temperature an entire series of partially relaxed line shapes are available for simulation rather than a single spectrum.

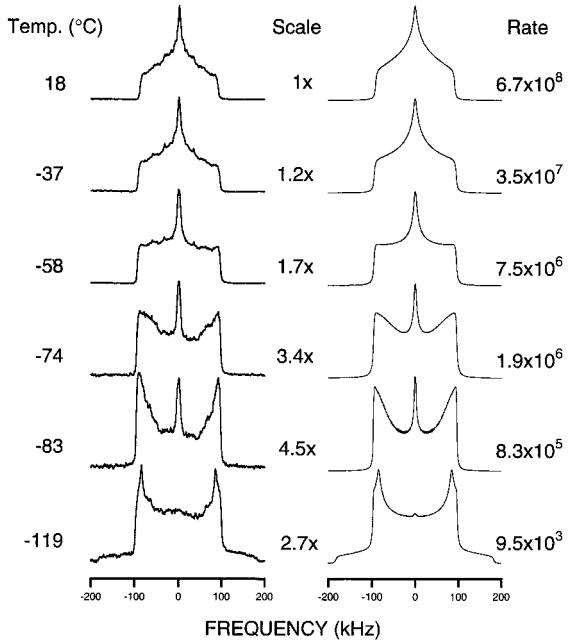

Figure 1. Temperature dependence of the experimental quadrupole echo spectra of $Ba(ClO_3)_2 \cdot {}^2H_2O$ and corresponding simulations for a pulse delay of $\tau = 30$ μs. The jump rates used in the simulation and the scaling of the intensities are as indicated.

The spectra displayed in Figure 1 are typical for the rigid, intermediate, and fast exchange limits and demonstrate the excellent agreement that can be achieved between the experimental and calculated line shapes. At −119 °C, using a recycle delay of 200 s, we obtain an almost rigid lattice line shape displaying an asymmetry parameter $\eta = 0.074$. In contrast, spectra recorded between −83 and −58 °C are characteristic of the intermediate exchange regime where the rigid lattice tensors of the water molecule are transformed to an averaged field gradient tensor by the 2-fold flipping motion. In comparison to the rigid lattice spectrum, the intermediate exchange line shapes show no parallel edges and concurrently a spike appears in the middle of the spectrum, which develops with increasing temperature. The components of the rigid lattice electric field gradient perpendicular to the plane of the water molecule ($V_\perp$) are not affected by the 2-fold flipping motion, but the averaged tensor element lying along the axis of motion (the bisector of the water molecule) is approximately zero and corresponds to the center of the spectrum. Since $\mathrm{Tr}(H_Q) = 0$, the third tensor element must be the negative of the element of the static field gradient ($-V_\perp$) that is not averaged by the jump process. Thus, $V_\perp$ and $-V_\perp$ correspond to the outer edges of the averaged spectrum. Between −37 and 18 °C the rates are in the rapid exchange limit for the quadrupole echoes and the line shapes show no changes at higher temperature except that the width of the spectra decreases slightly, reflecting further averaging of the electric field gradient tensor via vibration.[32]

To illustrate the τ-dependent quadrupole echo spectra, line shapes recorded for a pulse spacing of 30, 100, and 200 μs at a temperature of −74 °C are presented in Figure 2a. Despite a large change in pulse spacing, the alterations in line shapes due to anisotropic dephasing of transverse magnetization (in the intermediate exchange regime) are relatively minor. However, it can be readily observed that T_2 is longest if the magnetic field orientation is perpendicular (outer edges) or parallel (spike)

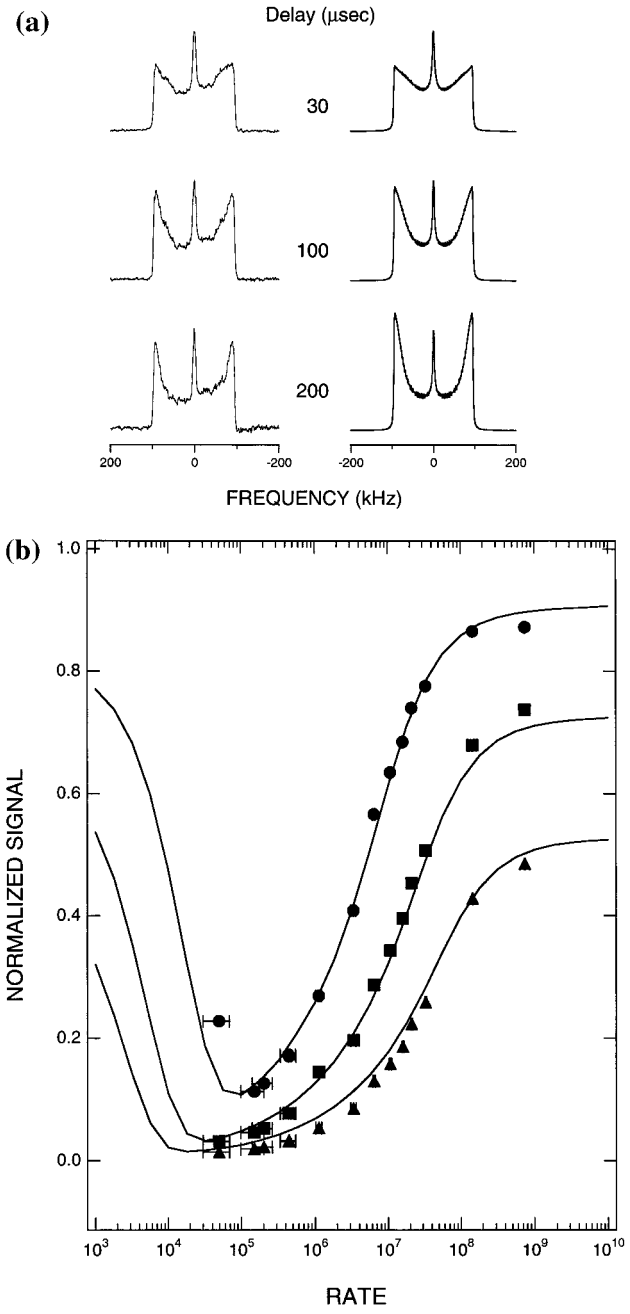

Figure 2. (a) τ-dependence of quadrupole echo spectra at a temperature of −74 °C. (b) Calculated (solid lines) and experimental signal intensities for three different pulse spacings: $\tau = 30$ (●), $\tau = 100$ (■), and $\tau = 200$ (▲) μs.

to the HOH bisector, while other orientations relax more quickly. The calculated line shapes in Figure 2a are in good agreement with the experimental spectra and describe the observed anisotropy. In a similar manner, the exchange-induced τ-dependence of the spectra can be interpreted.

Quadrupole Echo Spectral Intensities. In Figure 2a, all spectra have been scaled to the same intensity to ensure that details of the line shape may be observed. However, the tetrahedral jump model should not only account for changes in the line shape with τ and jump rate, but it should also predict the variation of signal intensity with temperature. For this reason we must compare experimental and calculated integrated signal intensities for a given value of τ at each temperature. The measurement of absolute signal intensities is complicated by the fact that a value for $\tau = 0$ is required, and this cannot be obtained because of the finite recovery time of the spectrometer components following the rf pulses. However, the absolute

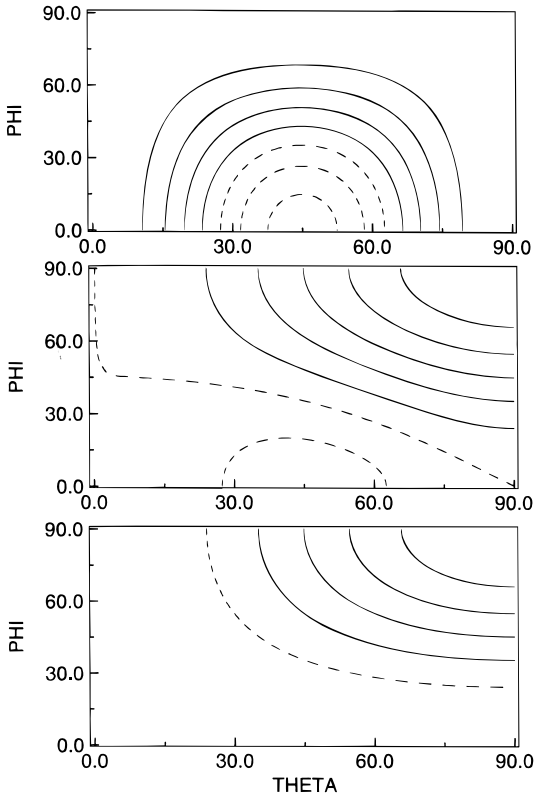

Figure 3. Contour plots representing the anisotropy of T_1 in which the angles θ and ϕ specify the magnetic field orientation in the molecular frame: (top) $k \ll \omega_0$; (middle) $k \approx \omega_0$; (bottom) $k \gg \omega_0$.

signal intensity can be measured in the rapid exchange limit where the echo intensity has an almost exponential dependence on τ; there, extrapolation of the points to $\tau = 0$ is possible. By correction of these intensities for temperature variations through use of the Boltzmann factor, $e^{-h\omega/(kT)}$, the desired fast limit echo intensities of the FID can be calculated. For the intermediate exchange regime, where relaxation is strongly orientation-dependent, this extrapolation of data points is not possible, since the transverse relaxation is very nonexponential. An additional consideration in calculating absolute echo intensities is the fact that finite pulse width effects are larger for a rigid lattice than for motionally averaged spectra, which may result in excessively low echo intensity measurements for $\tau_c^{-1} \ll \omega_Q$.

The solid lines in Figure 2b are calculated signal intensities for pulse spacings of 30, 100, and 200 μs on the basis of the two-site jump model for the water molecule assuming a fast-limit T_2 of 320 μs. Although this relaxation parameter does not change the line shape profile, it largely determines the echo intensity in the rigid and rapid exchange cases, since transverse relaxation in these limits is no longer dominated by modulation of the quadrupole interaction. This is particularly significant for longer pulse delays. In addition, finite pulse width effects lead to signal intensities of less than 1, since broad-band excitation of the spectra is limited. For short pulse spacing this contribution to the reduction of signal intensities may overshadow losses due to transverse relaxation, and losses are larger for the rigid exchange limit than for the fast exchange limit because of the broader spectral width for the static case. The jump rates for the experimental points were obtained by analyzing the corresponding inversion recovery spectra as discussed in the next section. The variation of the signal intensities shows that, in the rigid and fast limit regimes for the quadrupole echo experiment, significant attenuation of the echo is observed even though the line shapes are no longer dependent on the jump rates. Interestingly, the curves are

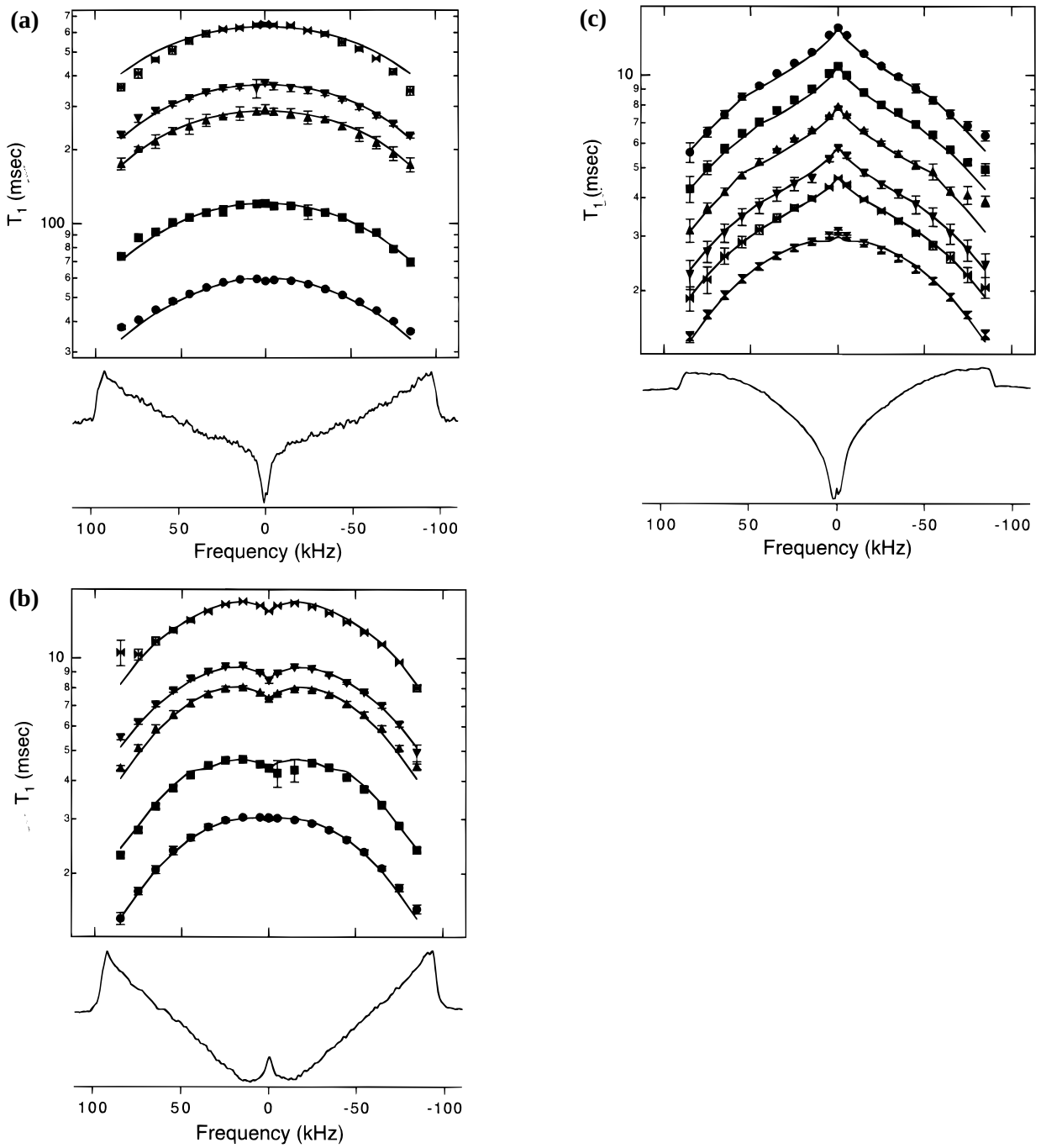

Figure 4. (a) Experimental and calculated T_1 anisotropy profiles at five different temperatures between −90 and −60 °C ($k \ll \omega_0$): (top curve) −89 °C, $k = 4.3 \times 10^5$; (▼) −83 °C, $k = 7.6 \times 10^5$; (▲) −81 °C, $k = 9.65 \times 10^5$; (■) −71 °C, $k = 2.4 \times 10^6$; (●) −62 °C, $k = 5.2 \times 10^6$. A spectrum taken near the T_1 zero crossing (230 ms) at −83 °C is also plotted. (b) Experimental and calculated T_1 anisotropy profiles at five different temperatures between −45 and −8 °C ($k \approx \omega_0$): (top curve) −44 °C, $k = 2.30 \times 10^7$; (▼) −37 °C, $k = 3.98 \times 10^7$; (▲) −34 °C, $k = 4.66 \times 10^7$; (■) −23.5 °C, $k = 8.75 \times 10^7$; (●) −8.4 °C, $k = 2.10 \times 10^8$. A spectrum taken near the T_1 zero crossing (5.5 ms) at −37 °C is also plotted. (c) Experimental and calculated T_1 anisotropy profiles at six different temperatures between 0 and 55 °C ($k \gg \omega_0$): (bottom curve) 1.0 °C, $k = 3.20 \times 10^8$; (second from bottom) 20.5 °C, $k = 6.92 \times 10^8$; (▼) 27.3 °C, $k = 9.45 \times 10^8$; (▲) 36.2 °C, $k = 1.34 \times 10^9$; (■) 45.6 °C, $k = 1.85 \times 10^9$; (●) 54.9 °C, $k = 2.48 \times 10^9$. A spectrum taken near the T_1 zero crossing (3.6 ms) at 36.2 °C is also plotted.

asymmetric with a minimum that is dependent on the pulse spacing. It is shifted to slower exchange rates with increasing pulse spacing. In particular, for a delay of 30 μs the minimum occurs at $\log(k) = 5$, with a signal intensity of about 11% of the FID intensity. The corresponding minima for the pulse spacings 100 and 200 μs occur at $\log(k) = 4.5$ and 4.2, with signal intensities of 3% and less than 1%, respectively. The comparison of experimental and calculated signal intensities shows good agreement. We did not measure signal intensities for rates below $\log(k) = 4.5$, since the relaxation time T_1 becomes prohibitively long.

Anisotropic Spin−Lattice Relaxation. In addition to quadrupole echo line shapes, we have employed the anisotropy of the deuteron spin−lattice relaxation to determine the rates of motion. Before discussing line shapes for partially recovered spectra recorded as a function of temperature, we examine the orientation dependence of T_1 (Figure 3). As usual, the spherical polar angles, θ and ϕ, define the orientation of the external magnetic field in the molecular frame. Note that the orientations with longer T_1's are shown by dotted contours, while the faster relaxing orientations are indicated by solid lines. These contours were generated using correlation functions for two-site 180°

flips.[34] The Zeeman relaxation is dominated by motions of the quadrupole nucleus on the order of the Larmor frequency and twice the Larmor frequency,

$$\frac{1}{T_{1z}} = \frac{3\pi^2}{2}(e^2qQ/h)^2[J_1(\omega_0) + 4J_2(2\omega_0)] \quad (1)$$

For two equivalent sites, the correlation functions, assuming $\eta = 0$, are

$$J_1(\omega_0) = \frac{1}{2}\frac{3k}{4k^2 + \omega_0^2}\sin^2\beta\cos^2\beta[1 - 3\cos^2\theta + 4\cos^4\theta + (4\cos^4\theta - 5\cos^2\theta + 1)\cos 2\phi] \quad (2)$$

$$J_2(2\omega_0) = \frac{1}{2}\frac{3k}{4k^2 + 4\omega_0^2}\sin^2\beta\cos^2\beta[1 - \cos^4\theta - \sin^4\theta\cos 2\phi] \quad (3)$$

where β is the angle between the O−D bond and the flipping axis. For tetrahedral geometry, this angle is near the magic angle (54.75°). In the top plot of Figure 3, $k \ll \omega_0$, so the expression for the correlation functions reduces to

$$J_1(\omega_0) + 4J_2(2\omega_0) = \frac{3k}{2\omega_0^2}\left[1 - \frac{3}{2}\cos^2\theta(1 - \cos^2\theta)(1 + \cos 2\phi)\right] \quad (4)$$

If the hopping rate is equivalent to the Larmor frequency,

$$J_1(\omega_0) + 4J_2(2\omega_0) = \frac{5}{6k}\left[1 - \frac{3}{5}\cos^2\theta + \frac{3}{10}(\cos^4\theta - 1)(1 + \cos 2\phi)\right] \quad (5)$$

This result is plotted in the middle of Figure 3. Since the rate increases until it is much greater than the Larmor frequency, the relaxation follows

$$J_1(\omega_0) + 4J_2(2\omega_0) = \frac{3}{8k}\left[1 - \frac{3}{2}\sin^2\theta(1 - \cos 2\phi)\right] \quad (6)$$

as shown in the bottom plot of Figure 3.

To understand the effect of orientation-dependent T_1's on the partially relaxed line shapes, it is necessary to relate the tensor elements $V_{||}$ and $V_\perp$ to their spectral frequencies. In the case of the motionally averaged asymmetric $\eta = 1$ spectrum, the elements $\pm V_\perp$ ($\theta = 90°$, $\phi = 0°$, 90°) define the outer portion of the spectrum, while $V_{||}$ ($\theta = 0°$) generates the center of the spectrum. Next, we consider the T_1 anisotropy for three cases with jump rate $k \ll \omega_0$ (Figure 3, top), $k = \omega_0$ (middle), and $k \gg \omega_0$ (bottom). For jump rates much slower than the Larmor frequency, T_1 is longest if $\theta = 45°$ and $\phi = 0°$, while the shortest T_1 is given by orientations where $\theta = 0°$ or $\theta = 90°$. Thus, the portions of the spectrum determined by $\pm V_\perp$ and $V_{||}$ should recover first. In the middle frame of Figure 3 the jump rate is comparable to the Larmor frequency and characteristics of the T_1 anisotropy of the slow and fast regimes are superimposed. Examining the bottom contour plot, we see that the T_1 anisotropy is distinctly different for jump rates faster than the Larmor frequency. Again, T_1 is shortest if $\theta = 90°$, $\phi = 90°$, reflecting the tensor element $V_\perp$ that is not averaged by the molecular motion. However, in this regime T_1 is longest for $V_{||}$ (center of the spectrum). Consequently, a reversal in the anisotropy of the powder pattern will be observed upon going from $k \ll \omega_0$ to $k \gg \omega_0$.

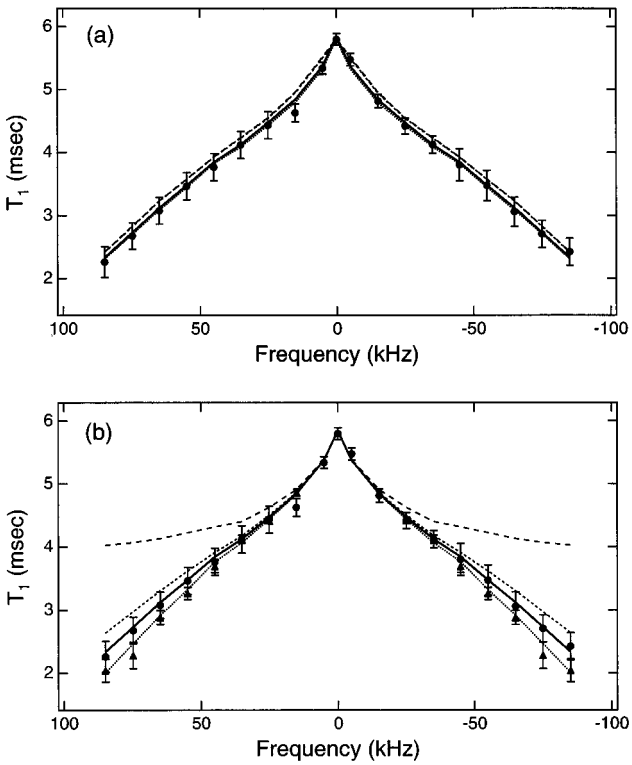

Figure 5. (a) Experimental and calculated T_1 anisotropy profiles at 27.3°: (●) experimental data; (···) $k = 9.45 \times 10^8$, $e^2qQ/h = 231.4$ kHz, $\eta = 0.040$; (−) $k = 9.76 \times 10^8$, $e^2qQ/h = 231.4$ kHz, $\eta = 0$; (- - -) $k = 1.07 \times 10^9$, $e^2qQ/h = 243.5$ kHz, $\eta = 0.074$; (− − −) $k = 1.14 \times 10^9$, $e^2qQ/h = 243.5$ kHz, $\eta = 0$. (b) Experimental and calculated T_1 anisotropy profiles at 27.3°: (●) experimental data with inversion pulse length of 4.0 μs; (▲) experimental data with inversion pulse length of 4.4 μs; (···) $k = 9.45 \times 10^8$, pulse width correction of 4.4 μs; (−) $k = 9.45 \times 10^8$, pulse width correction of 4.0 μs; (- - -) $k = 9.45 \times 10^8$, pulse width correction of 3.6 μs; (− − −) $k = 9.45 \times 10^8$, no pulse width correction.

We now examine the experimental and calculated T_1's measured via inversion recovery experiments at several different temperatures. The T_1's in Figure 4a were measured between −90 and −60 °C where $k \ll \omega_0$. Discounting finite pulse width effects (discussed below), little anisotropy is seen in the frequency profile. However, if individual spectra taken near the zero-crossing are examined, it is still possible to see significant anisotropy. Such a spectrum is plotted at the bottom of Figure 4a. In parts b and c of Figure 4 T_1's were measured in the ranges −45 to −8 °C and 1 to 55 °C, respectively. These correspond to jump rates with $k \approx \omega_0$ and $k \gg \omega_0$. Observed and simulated relaxation rates are in excellent agreement for all temperatures. In particular, it is possible to see the reversal in the anisotropy at the center of the spectra as the hopping rate increases, and for the rapid exchange limit $k \gg \omega_0$, the center of the spectrum exhibits a relatively long T_1 in accordance with our predictions from the anisotropic relaxation profiles in Figure 3. Examination of spectra taken near the zero-crossing at −37 °C and 36.2 °C (parts b and c of Figure 4, respectively) also demonstrates this reversal of anisotropy at the center frequency.

Finally, in this section we will discuss the dependence of the relaxation simulations on vibrational averaging of the quadrupole coupling constant and η as well as finite pulse width corrections. In Figure 5a the relaxation observed at room temperature is plotted along with best-fit simulations using the rigid-lattice and vibrationally averaged quadrupole coupling constants both including and neglecting the contributions of $\eta \neq 0$ to the correlation functions. Within experimental error these simula-

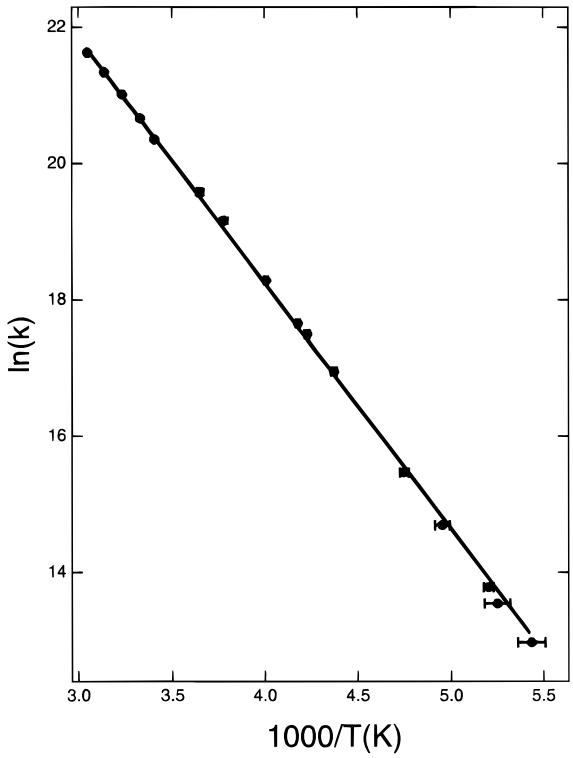

Figure 6. Observed temperature dependence of the jump rate for the 180° flipping motion of the water molecule. A least-squares fit of the data yields an activation energy of 29.9 ± 0.9 kJ/mol.

tions are indistinguishable. However, the hopping rates vary significantly from 9.45×10^8 using the vibrationally averaged constants to 1.14×10^9 using the rigid lattice quadrupole coupling and $\eta = 0$. In fact neglecting either of these parameters, the averaging of the quadrupole coupling or the inclusion of $\eta \neq 0$ in the calculation of the correlation function, can lead to a 5% error in the determination of the activation energy for the hopping, and their effects are additive (data not shown). Figure 5b demonstrates the effect of incomplete inversion due to finite pulse widths. Experimental data for inversion pulse lengths of 4.0 and 4.4 μs agree well with simulation results. In addition, the expected results for 3.6 μs and complete inversion are shown.

Activation Energy for Reorientation of the Hydrate Molecule. The rates of chemical exchange obtained by simulating the inversion recovery profiles are plotted in the form of $\ln k$ versus $1/T$ in order to obtain the activation energy for the rotation of the water molecule about its C_2 axis. The points fall almost on a straight line between rates of 4.3×10^5 and 2.48×10^9 s^{-1}. (Note that the point at a temperature of −119 °C was obtained by extrapolation, yielding the jump rate that was used to simulate the low-temperature spectrum in Figure 1.) The plot presented in Figure 6 is consistent with an activation energy of 29.9 ± 0.9 kJ/mol. If we assume that each water deuteron is linked by a hydrogen bond to the nearest oxygen atom of the chlorate anion, then the 180° flip motion involves breaking two hydrogen bonds. The activation energy calculated for $Ba(ClO_3)_2 \cdot H_2O$ is typical for hydrates with hydrogen bonds of moderate strength if crossing the rotational barrier is associated with breaking the hydrogen bonds.[27,30] In barium chlorate monohydrate the hydrogen bond has a length of 1.991 Å as measured by neutron scattering, which is typical for an N−D···O bond.[33] In further support of our measurement, the activation energy reported here is in good agreement with values reported by other NMR techniques. In particular, proton spin−lattice relaxation time measurements on single crystals of $Ba(ClO_3)_2 \cdot H_2O$ provided an activation energy of 19.2 ± 2.1 kJ/mol[30] (the isotope effect due to the substitution of deuterium predicts a ratio of 1.4 for the activation energies.), while CW deuteron line shape analysis performed on single crystals of $Ba(ClO_3)_2 \cdot D_2O$ yielded an activation energy of 27.2 kJ/mol.[31]

Conclusions

Deuterium NMR spectroscopy has been employed to investigate the motion of the water molecule in barium chlorate monohydrate. A simple two-site jump model describing exchange between degenerate orientations has been demonstrated to provide excellent agreement between experimental and simulated quadrupole echo and inversion recovery spectra. In the temperature range considered in this work, lattice vibration and internal vibratory motions of the water molecule need not be explicitly included in the calculation of the longitudinal relaxation time T_1, but they do lead to averaging of the quadrupolar coupling and η.

Motions with rates higher than the quadrupole coupling constant can be studied conveniently by the inversion recovery sequence, while motions with rates on the order of or slower than the coupling constant may also be determined using the τ-dependence technique. Thus, the combination of quadrupole echo and inversion recovery measurements, with iterative simulations of the data, provides an excellent tool for probing the mechanism and time scale of molecular motions in solids.

Acknowledgment. J. R. Long is the recipient of a National Science Foundation predoctoral fellowship. This work was supported by the National Institutes of Health (GM-25505, GM-23289, and RR-00995).

References and Notes

(1) Griffin, R. G., *Methods Enzymol.* **1981**, *72*, 108−174.
(2) Davis, J. H. *Biochim. Biophys. Acta* **1983**, *737*, 117−171.
(3) Griffin, R. G.; Beshah, K.; Ebelhauser, R.; Huang, T. H.; Olejniczak, E. T.; Rice, D. M.; Siminovitch, D. J.; Wittebort, R. J. In *The Time Domain in Surface and Structural Dynamics*; Long, G. J., Grandjean, F., Eds.; Kluwer Academic Publishers: Dordrecht, 1988; pp 81−105.
(4) Vega, A. J.; Luz, Z. *J. Chem. Phys.* **1987**, *86*, 1803−1813.
(5) Spiess, H. W.; Sillescu, H. *J. Magn. Reson.* **1981**, *42*, 381−389.
(6) Spiess, H. W. In *Dynamic NMR Spectroscopy*; Springer-Verlag: Berlin, 1978; Vol. 15, pp 55−214.
(7) Torchia, D. A.; Szabo, A. *J. Magn. Reson.* **1982**, *49*, 107−121.
(8) Wittebort, R. J.; Olejniczak, E. T.; Griffin, R. G. *J. Chem. Phys.* **1987**, *86*, 5411−5420.
(9) Hiyama, Y.; Silverton, J. V.; Torchia, D. A.; Gerig, J. T.; Hammond, S. J. *J. Am. Chem. Soc.* **1986**, *108*, 2715−2723.
(10) Rice, D. M.; Meinwald, Y. C.; Scheraga, H. A.; Griffin, R. G. *J. Am. Chem. Soc.* **1987**, *109*, 1636−1640.
(11) Rice, D. M.; Wittebort, R. J.; Griffin, R. G.; Meirovitch, E.; Stimson, E. R.; Meinwald, Y. C.; Freed, J. H.; Scheraga, H. A. *J. Am. Chem. Soc.* **1981**, *103*, 7707−7710.
(12) Sarkar, S. K.; Young, P. E.; Torchia, D. A. *J. Am. Chem. Soc.* **1986**, *108*, 6459−6464.
(13) Batchelder, L. S.; Niu, C. H.; Torchia, D. A. *J. Am. Chem. Soc.* **1983**, *105*, 2228−2231.
(14) Beshah, K.; Olejniczak, E. T.; Griffin, R. G. *J. Chem. Phys.* **1987**, *86*, 4730−4736.
(15) Beshah, K.; Griffin, R. G. *J. Magn. Reson.* **1989**, *84*, 268−274.
(16) Long, J. R.; Sun, B.; Bowen, A. E.; Griffin. R. G. *J. Am. Chem. Soc.* **1994**, *116*, 11950−11956.
(17) Maus, D. C.; Copie, V.; Sun, B.; Griffiths, J. M.; Griffin, R. G.; Luo, S.; Schrock, R. R.; Liu, A. H.; Seidel, S. W.; Davis, W. M.; Grohmann, A. *J. Am. Chem. Soc.* **1996**, *118*, 5665−5671.
(18) Jelinski, L. W. *Annu. Rev. Mater. Sci.* **1985,** *15*, 359−377.
(19) Spiess, H. W. In *Advances in Polymer Science*; Kausch, H. H., Zachmann, H. G., Eds.; Springer-Verlag: Berlin, 1985; Vol. 66, pp 23−58.
(20) Spiess, H. W. *Colloid Polym. Sci.* **1983**, *261*, 193−209.
(21) Ebelhauser, R.; Spiess, H. W. *Ber. Bunsen-Ges. Phys. Chem.* **1985**, *89*, 1208−1214.
(22) Burke, P. A.; Griffin, R. G.; Klibanov, A. M. *Biotechnol. Bioeng.* **1993**, *42*, 87−94.

(23) Speyer, J. B.; Weber, R. T.; Das Gupta, S. K.; Griffin, R. G. *Biochemistry* **1989**, *28*, 9569−9574.

(24) Ruocco, M. J.; Siminovitch, D. J.; Long, J. R.; Das Gupta, S. K.; Griffin, R. G. *Biophys. J.* **1996**, *71*, 1776−1778.

(25) Siminovitch, D. J.; Ruocco, M. J.; Olejniczak, E. T.; Das Gupta, S. K.; Griffin, R. G. *Chem. Phys. Lett.* **1985**, *119*, 251−255.

(26) Huang, T. H.; Skarjune, R. P.; Wittebort, R. J.; Griffin, R. G.; Oldfield, E. *J. Am. Chem. Soc.* **1980**, *102*, 7377−7379.

(27) Holcomb, D. F.; Pedersen, B. *J. Chem. Phys.* **1962**, *36*, 3270−3273.

(28) McGrath, J. W.; Silvidi, A. A. *J. Chem. Phys.* **1963**, *39*, 3017−3021.

(29) Silvidi, A. A.; McGrath, J. W.; Holcomb, D. F. *J. Chem. Phys.* **1964**, *41*, 105−111.

(30) Silvidi, A. A. *J. Chem. Phys.* **1966**, *45*, 3892−3895.

(31) Chiba, T. *J. Chem. Phys.* **1963**, *39*, 947−953.

(32) Ericksson, A.; Hussein, N. A.; Berglund, B.; Tegenfeldt, J.; Lindren, J. *J. Mol. Struct.* **1979**, *52*, 95−105.

(33) Sikka, S. K.; Momin, S. N.; Rajagopal, H.; Chidambaram, R. *J. Chem. Phys.* **1968**, *48*, 1883−1890.

(34) Vold, R. R.; Vold, R. L. In *Advances in Magnetic and Optical Resonance*; W. Warren, Ed.; Academic Press, Inc.: San Diego, 1991; Vol. 16, pp 85−171.